Pramana – J. Phys. (2021) 95:110
https://doi.org/10.1007/s12043-021-02145-6

Relativistic configuration interaction and many-body perturbation theory of energy levels, wavelengths, oscillator strengths, radiative rates and lifetimes of He-like lithium

SOUMAYA MANAI[1,2,3] and HAIKEL JELASSI[1,2,*]

[1]Research Laboratory on Energy and Matter for Nuclear Sciences Development, LR16CNSTN02 Tunis, Tunisia
[2]National Center for Nuclear Sciences and Technologies, Sidi Thabet Technopark, 2020 Ariana, Tunisia
[3]Faculty of Sciences of Bizerte, University of Carthage, Tunis, Tunisia
*Corresponding author. E-mail: haikel.jelassi@gmail.com, haikel.jelassi@cnstn.rnrt.tn

MS received 26 October 2020; revised 10 February 2021; accepted 12 March 2021

Abstract. The aim of this work is to provide energy level calculations among the lowest 71 levels arising out of $1s^2$ and $1snl$ ($n \leq 6, l \leq (n-1)$) configurations of He-like lithium. The calculations are carried out through the relativistic configuration interaction approach and the second-order many-body perturbation theory implemented in the flexible atomic code. We provide accurate calculations of energy levels, lifetimes, wavelengths, weighted oscillator strengths and radiative rates for the allowed ($E1$) transitions of He-like lithium. We have also considered relativistic effects by incorporating quantum electrodynamics and Breit corrections. The radiative lifetimes are reported for all the calculated levels. The present results are in good agreement with the previous results in literature (theoretical and experimental data). Several new energy levels and wavelengths were found out where no other theoretical or experimental results are available. We expect that our extensive calculations will be useful to experimentalists for identifying the fine-structure levels.

Keywords. Energy levels; lifetimes; oscillator strengths; radiative rates; relativistic configuration interaction; many-body perturbation theory.

PACS Nos 95.30.Ky; 32.70.Cs

1. Introduction

New and accurate atomic data for energy levels, lifetimes, wavelengths, oscillator strengths and radiative rates are required for the modelling of plasmas, such as in astrophysical media and nuclear fusion [1,2]. Importantly, transition data of low Z atoms can be used in the determination of element abundances and plasma diagnostics [3,4]. For instance, with the ongoing International Thermonuclear Experimental Reactor (ITER) project [5,6], there is a need for more accurate atomic data for a wide range of ions. Low Z He-like ions have been attractive subjects of theoretical and experimental investigations. Even though they are the simplest few-body systems, He-like ions are the most important atomic species in high-temperature astrophysical and laboratory sources. Emission lines of He-like ions have been widely observed in astrophysical and laboratory plasma environments [7]. Previously, Dere *et al* [8] provided a list of many detected He-like ion lines in solar plasmas at X-ray wavelengths region (1–50 Å).

Several studies targeting Li II, the second member of the helium isoelectronic sequence, have been performed. Indeed, the choice of this ion (Li II) is not random. In fact, one of the main challenges of ITER [9] is to produce tritium, as raw material for fusion, from a lithium source. Lithium is one of the most promising candidates for the fusion reaction [10].

Experimentally, Cantu *et al* [11] have detected many lines of Li II in the 160–215 Å range in laboratory plasmas. Energy levels, wavelengths and transition probabilities have been compiled and published in the NIST database [12].

Electronic supplementary material: The online version of this article (https://doi.org/10.1007/s12043-021-02145-6) contains supplementary material, which is available to authorized users.

Published online: 01 July 2021

Diehl *et al* [13] have measured the angle-resolved energy dependence of the electrons emitted over the energy range of the triply excited $2s^2 2p^2\,P$ lithium resonance using synchrotron radiation. In the theoretical side, Drake [14] has presented oscillator strengths for some dominant transitions of He and He-like ions using the Hylleraas–Scherr–Knight variation-perturbation method. Zhou and Manson [15] have performed R-matrix calculations of the photoionisation of the core-excited $1s2s2p^4\,P^{\mathrm{o}}$ state of atomic lithium. Głowacki Leszek [16] has calculated the excitation energy and the oscillator strength values for the $1s^2$–$1s2p$, $1s2s$–$1s2p$, $1s2s$–$1s3p$ transitions in the He isoelectronic sequence ($Z = 2$ through $Z = 116$). Wijngaarden and Jian [17] have employed novel spectroscopic techniques to precisely measure the fine and hyperfine structure splittings as well as the isotope shifts for several transitions at optical frequencies for the stable ^{6,7}Li and radioactive isotopes ^{8,9,11}Li.

Sow *et al* [18] have calculated the energy levels of atoms and ions with $2 \le Z \le 15$ using a Hyllerass approximation. The most recent calculation for these ions has been done by Aggarwal *et al* [19]. They have calculated energy levels, lifetimes, wavelengths, weighted oscillator strengths and transition rates of He-like Li up to $n = 5$. Our target is to extend the calculation and present a complete and accurate data for this ion. We expect that our extensive calculations will be useful to experimentalists to identify fine-structure levels.

In fact, we extend the calculations up to the $n = 6$ complex using the flexible atomic code (FAC) [20], for the determination of atomic parameters such as energy levels, wavelengths, oscillator strengths, radiative rates and lifetimes. This work focusses on the lowest 71 fine-structure levels and the allowed transitions ($E1$), arising out of ($n \le 6, l \le (n-1)$) configurations of He-like lithium. Other relativistic corrections deriving from the Breit interaction and quantum electrodynamics (QED) effects (vacuum polarisation and Lamb shift) are also included.

For this purpose, we employed three approaches implementing in the FAC code of Gu [20] namely, FAC, relativistic configuration interaction (RCI) and many-body perturbation theory (MBPT). In order to reach higher accuracy, both RCI and MBPT calculations were performed using an extended atomic basis including levels belonging to complexes till $n = 20$ complexes. The present results are then compared with the available experimental [12] and theoretical results [17].

First, we review the theoretical background used by the FAC code. Second, the computational details of the calculation of the $1s^2$, $1s2l$, $1s3l$, $1s4l$, $1s5l$ and $1s6l$ configurations of He-like Li which give rise to the lowest 71 fine-structure levels, are presented. The number of levels of the fine structure which we considered is larger than any other theoretical calculations. Then, our set of data composed of energy of lowest 71 levels in cm^{-1} and their corresponding lifetimes τ (s), wavelengths λ (Å), weighted oscillator strengths $g_i f_{ij}$ (dimensionless) and radiative rates A_{ij} (s^{-1}), for 462 allowed $E1$ transitions and obtained by each method, are presented. Finally, a discussion of our results and comparisons with the available theoretical and experimental data are presented.

2. Theoretical method

FAC is a highly efficient fully relativistic code created by Ming Feng Gu [20] which enables the user to carry out large-scale computations and allows finding various atomic parameters. We employed the version 1.1.4 of FAC to perform three different calculations namely, FAC, RCI and MBPT.

2.1 *FAC*

The relativistic Hamiltonian (H) for an atomic ion with N electrons (in atomic units) is [21,22]

$$H = \sum_{i=1}^{N} H_{\mathrm{D}}(i) + \sum_{i<j}^{N} \frac{1}{r_{ij}}, \tag{1}$$

where $H_{\mathrm{D}}(i)$ is the single-electron Dirac Hamiltonian due to nuclear charge potential. The approximate atomic state functions are given by mixing the basis states Φ_v with the same symmetries:

$$\psi = \sum_{v} b_v \Phi_v, \tag{2}$$

where b_v are the mixing coefficients obtained from diagonalising the total Hamiltonian [21]. We can write φ_{nkm} as

$$\varphi_{nkm} = \frac{1}{r} \begin{pmatrix} i P_{nk}(r)\chi_{km}(\theta,\phi,\sigma) \\ Q_{nk}(r)\chi_{km}(\theta,\phi,\sigma) \end{pmatrix}, \tag{3}$$

where k is the magnetic quantum momentum which is equal to $(l-j)(2j+1)$, m is the magnetic quantum number, n is the principal quantum number, $P_{n\kappa}(r)$ and $Q_{n\kappa}(r)$ are the large and small components, respectively and $\chi_{\kappa m}(r)$ is the spin angular function.

2.2 *RCI*

The many-electron Dirac Hamiltonian commonly used in RCI calculations [23] is

$$H_{\mathrm{Dirac}} = \sum_{i} h_0(i) + \sum_{i>j} \left[V_{\mathrm{C}}(ij) + V_{\mathrm{B}}(ij) \right], \tag{4}$$

where $h_0 = c\boldsymbol{\alpha} \cdot \mathbf{p} + (\beta - 1)c^2 + V_{\text{nuc}}(r)$ is the Dirac Hamiltonian of an electron, $V_{\text{C}}(ij) = 1/r_{ij}$ is the Coulomb interaction between the electrons, $V_{\text{B}}(ij) = B_{ij}$ is the frequency-independent Breit interaction given by [24]

$$B_{ij} = -\sum_{i<j}^{N} \frac{1}{2r_{ij}} \left[\alpha_i \cdot \alpha_j + \frac{(\alpha_i \cdot r_{ij})(\alpha_j \cdot r_{ij})}{r_{ij}^2} \right]. \quad (5)$$

2.3 *MBPT*

The MBPT method has been included within the FAC code and successfully used in calculating atomic parameters of high accuracy. In the MBPT calculation, the no-pair Dirac–Coulomb–Breit (DCB) Hamiltonian for an N-electron ionic system is given by [25]

$$H_{\text{DCB}} = \sum_i \left[h_{\text{d}}(i) - \frac{Z}{r_i} \right] + \sum_{i<j} \left(\frac{1}{r_{ij}} + B_{ij} \right), \quad (6)$$

where h_{d} is the free-electron Dirac Hamiltonian, r_i is the radial coordinate of the electron i, r_{ij} is the distance between the electrons i and j and Z is the nuclear charge number.

The H_{DCB} Hamiltonian is split into H_0 as a model Hamiltonian and V as a perturbation [26]

$$H_0 = \sum_i = [h_{\text{d}}(i) + U(r_i)], \quad (7)$$

$$V = -\sum_i \left[\frac{z}{r_i} + U(r_i) \right] + \sum_i \frac{z}{r_i} + B_{ij}, \quad (8)$$

where $U(r)$ is a model potential including the screening effects of all electrons, which is approximated by a local central potential derived from Dirac–Fock–Slater self-consistent field calculation. It should be chosen appropriately to make the perturbation potential V as small as possible.

3. Computational details

As mentioned above, we employed FAC code to perform three different calculations: FAC, RCI and MBPT. We have performed a series of calculations up to $n = 6$, which generate 71 levels arising out of $1s^2$ and $1snl$ ($n \leq 6, l \leq (n-1)$) configurations of He-like Li.

For the first calculation, the code proceeds to the diagonalisation of the Hamiltonian (H) with no account to any configuration interaction among different complex n. For the RCI method, the configuration mixing approximation is used to calculate the bond states system with a specific mixing scheme. The local central potential is derived by a modified self-consistent Dirac–Fock–Slater iteration. Then, the derived local central potential is used to derive radial orbitals for the construction of basis states. Through the diagonalisation of the relativistic Hamiltonian, a procedural correction is applied to reduce errors in energy levels. For an ion with N electrons, relativistic Hamiltonian is constructed by summing over the single electron Dirac Hamiltonian due to contributions of the nuclear charge potential and the electron–electron interaction potential.

The main idea of the MBPT approach is to divide the Hilbert space of the full Hamiltonian into two orthogonal spaces, $\mathcal{M}$ and $\mathcal{N}$. In such a model, the $\mathcal{M}$ space represents a model space which contains the non-Hermitian effective Hamiltonian while $\mathcal{N}$ is a model space with perturbation expansion. The eigenvalues of this effective Hamiltonian yield energy levels of the full Hamiltonian. Once applied, the multi configuration interaction effects within the model space are exactly accounted, then the interaction between the $\mathcal{M}$ and $\mathcal{N}$ model spaces is calculated by the perturbation method. In our case, the model space $\mathcal{M}$ contains all the configurations we are interested in, i.e. all possible configurations of $1snl$ (n =1–6, l = 0–5). The orthogonal space $\mathcal{N}$ contains all configurations that are formed by single and double excitations from the $\mathcal{M}$ space. In our case, the space $\mathcal{N}$ contains configurations of $1snl$ (n = 7–20, $0 \leq l \leq n-1$). In addition, we have performed the RCI calculations using the same code FAC to assess the improvement of MBPT corrections. In RCI calculation, the electron correlations among the configurations included in the $\mathcal{M}$ model space of the above MBPT calculation are taken into account. In addition, in our present MBPT and RCI calculations, we also include several small corrections to the Hamiltonian H_{DBC} of eq. (6), such as the finite nuclear size (by using the nuclear potential for a finite hard sphere), vacuum polarisation (VP) (by including the Uehling potential), nuclear recoil (by adding the corresponding matrix elements to the Hamiltonian H_{DBC}) and the electron self-energy (SE) are calculated with a screened hydrogenic formula.

4. Results and discussion

4.1 *Energy levels*

In table S1 (given as the supplementary material), we summarise the energy levels of the lowest 71 levels of the He-like Li, obtained from FAC, RCI and MBPT calculations. Within the same table, we also compare them with experimental energies compiled by NIST [12] as well as theoretical calculations carried out by Aggarwal *et al* [19].

According to table S1, our values of energy levels obtained using the three methods are generally in good agreement against each other. Majority of values of energy levels obtained with FAC are consistently larger than the experimental ones by approximately 8000 cm^{-1}. The use of the RCI method allows improvement of the energy level determination. Indeed, the majority of values of energy levels are decreased by approximately 5000 cm^{-1}. The use of the MBPT approach significantly improves the value of the energy levels. As a result, the differences with the experimental values considerably decrease. The maximum difference relative to the NIST data becomes 651 cm^{-1}.

To compare our three calculations, we plot figure 1, in which we represent the calculated energy levels by the two methods FAC and RCI as a function of energy levels calculated by MBPT for 71 lowest levels arising out of $n \leq 6$, $l \leq (n-1)$ configurations of He-like Li. To compare the data, we add to figure 1, the first bisector, i.e. $x = y$, as well as two lines presenting $\pm 2\%$ with respect to the first bisector. The values of energy levels calculated by RCI (open square) are more aligned than those calculated by FAC (star). The relative deviation obtained is around 0.1% for the RCI method and 1% for the FAC calculation method. However, our two computational methods RCI and MBPT yield higher energy values than the values calculated by FAC method.

To further confirm the reliability of our results, we plotted in figure 2, the relative deviation of our energy levels obtained by the three different methods (FAC, RCI and MBPT) and energy levels obtained by Aggarwal *et al* as a function of the level index. All the relative deviations are calculated relatively to the experimental energy data extracted from the NIST database [12]. We present the relative deviation between our different methods and the experimental data by the following equation:

$$[(E_{\text{theory}} - E_{\text{NIST}})/E_{\text{NIST}}] \times 100.$$

The average relative deviation difference does not exceed $\pm 0.1\%$ for all the three methods compared to the NIST results. We obtained by the method FAC, $1.3 \pm 0.24\%$. With the same method, Aggarwal *et al* [19] obtained data with discrepancy of $1.48 \pm 0.32\%$. The use of the RCI method allows improvement of the energy level determination. Indeed, the average relative deviation is decreased in the range of $0.46 \pm 0.11\%$ with the MBPT method. The use of the MBPT approach significantly improves the value of the energy levels. As a result, the differences with the experimental values considerably decrease. The average relative deviation to the NIST data becomes $0.04 \pm 0.06\%$. It is important to mention that the energy level calculations performed by the MBPT method are the closest to the NIST data [12]. It should be noted that we have improved the existing

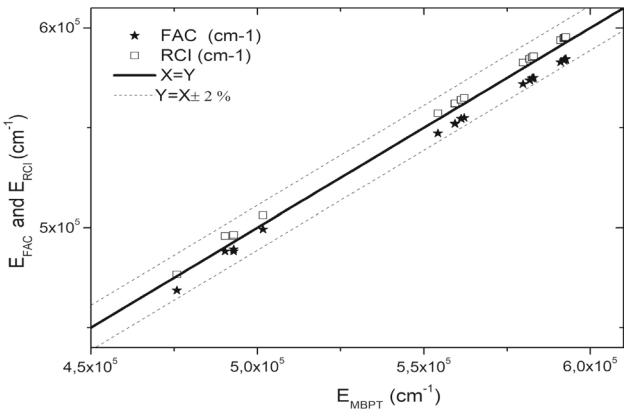

Figure 1. Energy levels calculated by the two methods (FAC and RCI) as a function of energy levels calculated by MBPT for the 71 lowest levels arising out of $n \leq 6$, $l \leq (n-1)$ configurations of He-like Li. The dashed lines lines present $\pm 2\%$ compared to the first bisector $x = y$.

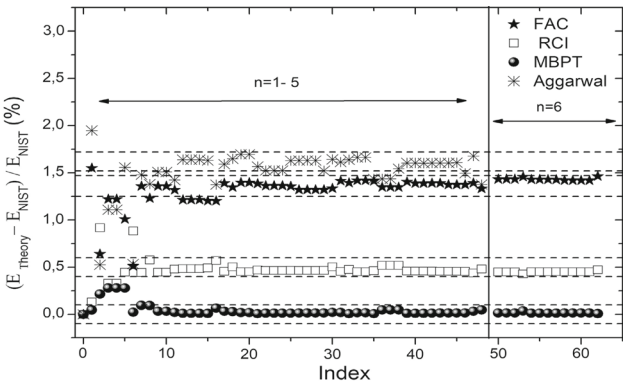

Figure 2. Relative deviations of the energy levels calculated by three different methods (FAC, RCI and MBPT) compared to the experimental values extracted from NIST [12], for the 71 lowest levels generated by the configurations $n \leq 6$, $l \leq (n-1)$ of He-like Li as a function of the level index. The data published in [19] by Aggarwal *et al* are also reported. The dotted lines present $\pm 0.1\%$ compared to the NIST results.

data for energy levels ($n = 5$) and the energy levels of the $n = 6$ complex are published for the first time.

4.2 *Wavelengths*

We start by presenting the wavelength values for electric dipole transitions ($E1$) values arising from $n \leq 6$, $l \leq (n-1)$ configurations of He-like Li, that we have calculated using the three methods mentioned above. We compare our computed 462 values of wavelengths with those provided by the NIST database (table S2, given as the supplementary material).

Table 1. Wavelengths in Å of a set of allowed ($E1$) transitions chosen arbitrarily, arising from $n \leq 6, l \leq (n-1)$ configurations of He-like Li and calculated by FAC, RCI and MBPT methods. Experimental data extracted from NIST database [12] as well as theoretical data calculated by Aggarwal *et al* [19] and ref. [27] are also presented.

i	j	λ_{FAC} (Å)	λ_{RCI} (Å)	λ_{MBPT} (Å)	$\lambda_{\text{Aggarwal}\,et\,al}$ (Å)	λ_{NIST} (Å) [12]	Others (Å) [27]
$1s2s\ ^3S_1$	$1s3p\ ^3P^o_1$	1215.07	1202.12	1198.44	1867.00	1198.09	–
$1s2p\ ^3P^o_2$	$1s3d\ ^3D_3$	1516.86	1511.57	1465.35	1511.00	1492.97	–
$1s2p\ ^1P^o_1$	$1s4s\ ^1S_0$	1347.61	1341.50	1248.47	1261.00	1253.8	1253.5
$1s3s\ ^3S_1$	$1s4p\ ^3P_2$	3735.42	3769.57	3632.04	3691.00	3684.32	–
$1s3p\ ^3P_2$	$1s4d\ ^3D_2$	4380.19	4393.93	4309.30	4366.00	4325.47	–
$1s2s\ ^3S_1$	$1s6p\ ^3P^o_1$	836.66	830.80	821.86	–	820.00	820.00
$1s2s\ ^3S_1$	$1s5p\ ^3P^o_2$	876.08	869.58	860.99	864.60	861.00	861.00
$1s2p\ ^3P^2_2$	$1s5s\ ^3S_1$	1061.88	1057.87	1019.30	1040.00	1032.00	1032.00
$1s2s\ ^3S_1$	$1s5p\ ^3P^o_0$	876.08	869.57	861.00	861.00	864.60	–
$1s2s\ ^3S_1$	$1s4p\ ^3P^o_1$	960.03	952.06	944.42	948.30	945.00	–
$1s2p\ ^3P^o_0$	$1s4d\ ^3D_1$	1160.75	1157.66	1116.13	1143.00	1132.10	1132.00
$1s2p\ ^3P^o_1$	$1s6d\ ^3D_2$	992.03	989.77	953.85	–	965.00	965.00
$1s3p\ ^3P^o_1$	$1s6d\ ^3S_1$	2728.07	2727.11	2653.78	–	2657.29	–
$1s3d\ ^3D_1$	$1s6f\ ^3F^o_2$	992.05	989.78	953.90	–	965.00	–
$1s2s\ ^1S_0$	$1s5p\ ^1P^o_1$	2861.81	2861.81	2732.40	–	2728.32	–
$1s2p\ ^3P^o_1$	$1s5d\ ^3D_2$	1045.72	1043.20	1005.30	1025.00	1018.00	–
$1s2s\ ^3P^o_1$	$1s5d\ ^3D_1$	1045.71	1043.20	1005.31	1027.00	1018.00	–
$1s2s\ ^3P^o_2$	$1s5d\ ^3D_3$	1045.73	1043.22	1005.36	1142.00	1018.00	–
$1s2p\ ^3P^o_1$	$1s5s\ ^3S_1$	1061.86	1057.86	1019.23	1040.00	1032.00	–
$1s2p\ ^3P^o_2$	$1s5s\ ^3S_1$	1061.88	1057.87	1019.30	1040.00	1032.00	–

i and j are the lower and upper levels of transition, respectively.

In table 1, we have only considered some of the allowed ($E1$) transition wavelengths calculated by the three proposed methods mentioned previously. In this table, the third column shows the wavelength values calculated by FAC, while the fourth and fifth columns are from RCI and MBPT, respectively. The last two columns are devoted to the experimental values extracted from the NIST database [12], and other references [27]. According to the values presented in table 1, it is clear that, our results are in good agreement with NIST determination [12] and Aggarwal *et al* [19].

For in-depth study, we present in figure 3, the relative deviation of wavelengths calculated by different methods (FAC, RCI and MBPT) as a function of NIST data [12].

We observe that the relative deviation does not exceed ±5% for the three calculations, except for six transitions, which are labelled in figure 3. We obtain for transitions $1s2p\ ^1P_3$–$1s5d\ ^1D_2$, $1s2s\ ^1S_0$–$1s3p\ ^1P^o_1$, $1s3d\ ^3D_3$–$1s4p\ ^3P^o_2$, $1s2p\ ^1P^o_1$–$1s3d\ ^1D_2$, $1s2p\ ^1P^o_1$–$1s3s\ ^1S_0$, $1s2s\ ^3S_1$–$1s2p\ ^3P^0_o$, relative deviations racing ±8%. By comparing the relative deviations for the three sets of calculation, we note that the MBPT calculation is the more accurate calculation. Indeed, the average relative deviation of MBPT method is $-0.47 \pm 0.9\%$, while averages of relative deviations for RCI and FAC calculations are $2.62 \pm 1.73\%$ and $3.13 \pm 1.66\%$, respectively.

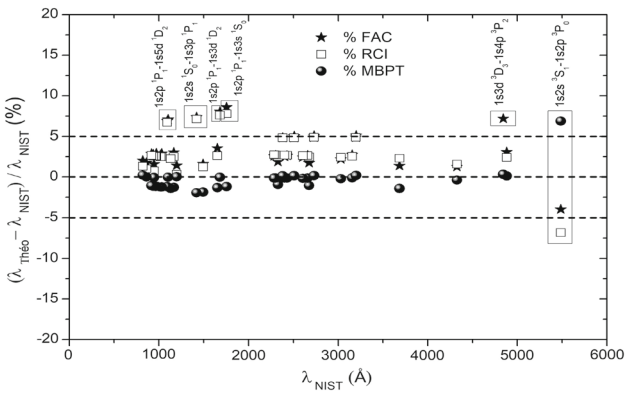

Figure 3. Relative deviations for wavelengths of the allowed ($E1$) transitions, arising from $n \leq 6, l \leq (n-1)$ configurations of He-like Li and calculated by different methods (FAC, RCI and MBPT). The relative deviations are plotted as a function of results obtained by NIST [12].

Table 2. Weighted oscillator strengths (dimensionless) and transition rates (in s^{-1}) for a selection of allowed ($E1$) transitions chosen arbitrarily, arising from $n \leq 6$.

i	j	FAC		RCI		MBPT		Aggarwal *et al*		NIST	
		gf	A (s^{-1})	gf	A (s^{-1})	gf	A (s^{-1})	gf	A (s^{-1})	gf	A (s^{-1})
$1s2p\ ^3P^o_2$	$1s3s\ ^3S_1$	1.59E−01	1.21E+08	1.54E−01	1.19E+08	1.63E−01	1.36E+08	1.82E−01	2.51E+07	1.95E−01	1.58E+08
$1s2s\ ^3S_1$	$1s3p\ ^3P^o_1$	2.68E−01	4.05E+08	1.49E−01	2.29E+08	1.80E−01	2.79E+08	1.09E−01	2.58E+07	1.87E−01	2.90E+08
$1s2s\ ^3S_1$	$1s3p\ ^3P^o_2$	4.47E−01	4.05E+08	2.48E−01	2.29E+08	3.00E−01	2.79E+08	3.82E−01	2.51E+07	3.12E−01	2.90E+08
$1s2s\ ^3S_1$	$1s3p\ ^3P^o_0$	1.20E−01	2.89E+07	1.11E−01	2.84E+07	1.01E−01	1.96E+07	1.87E−02	2.58E+08	1.03E−01	2.27E+07
$1s2p\ ^3P^o_1$	$1s3d\ ^3D_2$	1,59E+00	9,24E+08	1,31E+00	7,65E+08	1,42E+00	8,84E+08	4.73E−01	8.29E+08	1.40E+00	8,41E+08
$1s2p\ ^3P^o_2$	$1s3d\ ^3D_2$	5.31E−01	3.08E+08	4.36E−01	2.55E+08	4.74E−01	2.95E+08	9.47E−02	2.76E+08	4.68E−01	2.80E+08
$1s2p\ ^3P^o_2$	$1s3d\ ^3D_3$	2.97E+00	1.23E+09	2.44E+00	1.02E+09	2.65E+00	1.18E+09	2.65E+00	1.11E+09	2.62E+00	1.12E+09
$1s2p\ ^3P^o_1$	$1s3d\ ^3D_1$	5.31E−01	5.14E+08	4.36E−01	4.25E+08	4.74E−01	4.91E+08	4.73E−01	4.61E+08	4.68E−01	4.67E+08
$1s2p\ ^3P^o_2$	$1s3d\ ^3D_1$	3.54E−02	3.42E+07	2.91E−02	2.83E+07	3.16E−02	3.27E+07	3.16E−02	3.07E+07	3.12E−02	3.12E+07
$1s2p\ ^3P^o_0$	$1s3d\ ^3D_1$	7.08E−01	6.85E+08	5.82E−01	5.67E+08	6.31E−01	6.55E+08	8.12E−02	4.35E+04	6.25E−01	6.23E+08
$1s2p\ ^1P^o_1$	$1s3d\ ^1D_2$	1.77E+00	7.17E+08	2.14E+00	8.74E+08	2.24E+00	1.06E+09	7.40E−01	1.01E+09	2.13E+00	1.01E+09
$1s2s\ ^1S_0$	$1s3p\ ^1P^o_1$	2.14E−01	2.04E+08	2.65E−01	2.55E+08	2.60E−01	2.99E+08	1.03E+00	3.44E+08	2.57E−01	2.83E+08
$1s2p\ ^3P^o_1$	$1s4d\ ^3D_2$	2.83E−01	2.80E+08	2.60E−01	2.59E+08	2.74E−01	2.94E+08	4.53E−01	2.78E+08	2.77E−01	2.89E+08
$1s2p\ ^3P^o_2$	$1s4d\ ^3D_2$	9.43E−02	9.35E+07	8.66E−02	8.63E+07	9.13E−02	9.79E+07	9.07E−02	9.26E+07	9.24E−02	9.62E+07
$1s2p\ ^3P^o_2$	$1s4d\ ^3D_3$	5.28E−01	3.74E+08	4.84E−01	3.45E+08	5.11E−01	3.92E+08	3.05E−01	3.71E+08	5.18E−01	3.85E+08
$1s2p\ ^3P^o_1$	$1s4d\ ^3D_1$	9.43E−02	1.56E+08	8.65E−02	1.44E+08	9.13E−02	1.63E+08	1.51E−01	1.54E+08	9.24E−02	1.60E+08
$1s2p\ ^3P^o_2$	$1s4d\ ^3D_1$	6.28E−03	1.04E+07	5.77E−03	9.58E+06	6.09E−03	1.09E+07	1.21E−03	1.03E+07	6.16E−03	1.07E+07
$1s2p\ ^3P^o_0$	$1s4d\ ^3D_1$	1.26E−01	2.08E+08	1.15E−01	1.92E+08	1.22E−01	2.18E+08	2.56E+00	5.97E+07	1.23E−01	2.14E+08
$1s2p\ ^3P^o_2$	$1s5d\ \ ^3D_2$	3.46E−02	4.23E+07	3.14E−02	3.86E+07	3.32E−02	4.39E+07	3.15E−02	3.98E+07	3.51E−02	4.52E+07
$1s2p\ ^3P^o_2$	$1s6d\ ^3D_2$	1.69E−02	2.30E+07	1.41E−02	1.92E+07	1.52E−02	2.23E+07	–	–	1.75E−02	2.50E+07

$l \leq (n-1)$ configurations of He-like Li, calculated by FAC, RCI and MBPT. Experimental data from the NIST database [12] as well as results extracted from the theoretical reference works [19] are also represented. i and j are the lower and upper levels of the transition.

4.3 *Weighted oscillator strengths and transition rates*

The weighted oscillator strengths $g_i f_{ij}$ (dimensionless) are related to the transition rates A_{ji} (s^{-1}) and the wavelengths λ_{ji} for a transition from j to i by the following expression [28]:

$$g_i f_{ij} = \frac{mc}{8\pi^2 e^2}\lambda_{ji}^2 g_j A_{ji} = 1.49\times10^{-16}\lambda_{ji}^2 g_j A_{ji}, \quad (9)$$

where m and e are the electron mass and charge, respectively, c is the velocity of light, λ_{ji} is the wavelength in Å, g_i and g_j are the statistical weights of the lower (i) and upper (j) levels, respectively.

Table S3 (given as the supplementary material) summarises weighted oscillator strengths and transition rate values calculated by our different methods for the allowed ($E1$) transitions resulting from $n \leq 6$, $l \leq (n-1)$ configurations. In table S3, we also found for comparison, results of weighted oscillator strengths and transition rate values published in previous theoretical [19] and experimental [12] works.

In table 2, we have selected some values extracted from table S3. According to the values presented in table 2, one can easily confirm that our calculations are in good agreement. Referring to this set of data, our results are closer to the experimental results of NIST than the other theoretical results. Indeed, our values are much closer to the experiment than the values published by Aggarwal *et al* [19].

For an in-depth study, we present, in figure 4, the values of the weighted oscillator strengths for the allowed $E1$ transitions, calculated by FAC, RCI and MBPT as a function of the weighted oscillator strength values obtained by NIST. The values published in the NIST database have been weighted by g_i values of the lower levels of the transition. According to figure 4, all relative deviations do not exceed 3% (presented in figure 3 by $y = x \pm 3\%$ lines) for the three methods compared to the results from NIST database [12], except four transitions which are mentioned in figure 4: $1s4d\ ^3D_3$–$1s3p\ ^3P^o_2$, $1s6d\ ^3D_3$–$1s5p\ ^3P^o_2$, $1s5d\ ^3D_3$–$1s4p\ ^3P^o_2$ and $1s6p\ ^1P^o_1$–$1s6s\ ^1S_0$. Indeed, by comparing distances of the cloud of points for each method to the line $y = x$, we can state that relative deviation of MBPT's gf values to those extracted from the NIST database, are the smallest.

For low weighted oscillator strengths ($gf < 0.7$), the values are in good agreement, and the overall agreement among our results and the results of ref. [12] is good. The average deviations are within 1% for the MBPT calculation. The values obtained by RCI and FAC calculations are not very good compared to the MBPT values where the relative deviations reach 7.35% and 7.64% respectively. For $gf > 0.7$, the dispersion with respect to the

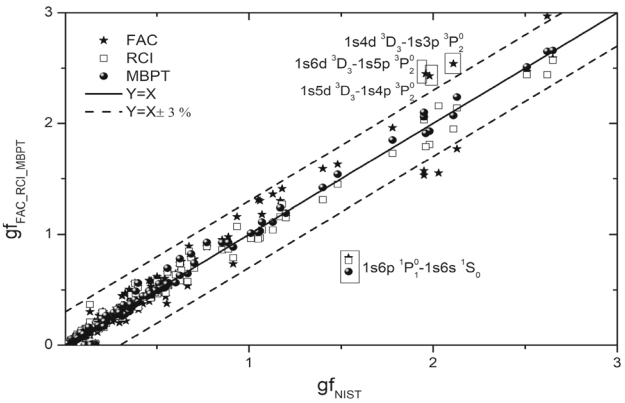

Figure 4. Values of weighted oscillator strengths of the allowed transitions, arising from $n \leq 6$, $l \leq (n-1)$ configurations of He-like Li, calculated by FAC, RCI and MBPT as a function of the values obtained by NIST database. The two dashed lines present ± 3% deviations compared to the first bisector.

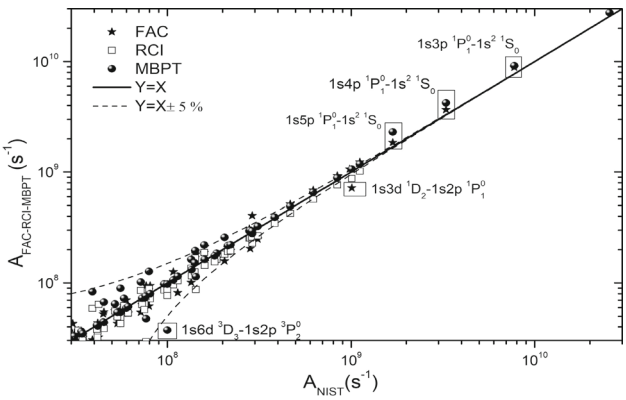

Figure 5. Values of radiative rates of the allowed transitions, arising from $n \leq 6$, $l \leq (n-1)$ configurations of He-like Li, calculated by FAC, RCI and MBPT as a function of the values obtained by NIST (log–log scale). The dashed lines present ± 5% deviations compared to the first bisector.

first bisector is more pronounced. The relative deviation for RCI and FAC calculations reaches 14%, while the relative difference of MBPT remains constant around 1%. In some cases, where transition is weak ($gf < 0.7$), this agreement may disappear, such as the $1s6p\ ^1P^o_1$–$1s6s\ ^1S_0$ and $1s4d\ ^3D_3$–$1s3p\ ^3P^o_2$ transitions.

We plot in figure 5, transition rates A_{ij} for the allowed ($E1$) transitions, calculated by different methods, as a function of experimental values [12]. The figure shows that the relative deviation of the majority of transitions does not exceed 5% except for five transitions which are $1s6d\ ^3D_3$–$1s2p\ ^3P^o_2$, $1s5p\ ^1P^o_1$–$1s^2\ ^1S_0$, $1s3d\ ^1D_2$–$1s2p\ ^1P^o_1$, $1s3p\ ^1P^o_1$–$1s^2\ ^1S_0$ and $1s4p\ ^1P^o_1$–$1s^2\ ^1S_0$.

For low values of transition rate, $A < 10^8$ (s^{-1}), our results remain in good agreement. Indeed, relative

deviation of the MBPT method agrees within 2.06% compared to the data from the NIST database. Values calculated by RCI and FAC approaches are not very good and their relative deviations reach 2.17% and 5.35%, respectively.

As the transition rates increase (i.e. $A > 10^8$ s^{-1}), the dispersion with respect to the first bisector is more pronounced. The relative deviation reaches 7.71% for RCI method and 9.7% for FAC method, while the relative deviation of MBPT remains almost constant at 2.13%.

4.4 *Lifetimes*

We are interested to calculate lifetimes of the 71 fine levels, arising from $n \leq 6, l \leq (n-1)$ configurations of He-like Li by FAC, RCI and MBPT methods.

The lifetime τ for a level j is defined as follows [29]:

$$\tau_j = \frac{1}{\sum_i A_{ji}}. \tag{10}$$

According to table S4 (given as the supplementary material), it is important to notify that our calculations are in good agreement with each other. Indeed, we also compare our values with values published by Aggarwal *et al* [19]. We find that our results are in excellent agreement with the theoretical data. It should be mentioned that the ground state does not have lifetime. The last column of the table presents experimental determinations of lifetimes from refs [17,30]. It is clear that our calculations are in good agreement with those experimental determinations. We found lifetimes of $1s2s^3S_1$ and $1s2s^1S_0$ worth 10^{+1} and 10^{+5} respectively, which are both metastable states of He-like Li.

5. Conclusion

In this work, we have presented our results obtained by the application of the FAC code using three different methods in order to generate a complete and accurate atomic data of the 71 energy levels of the $n \leq 6, l \leq (n-1)$ configurations of He-like Li. Using these energy levels, we calculated all the atomic data (wavelengths, oscillator strengths, radiative rates and lifetimes). The self-consistent field approximation and the Hamiltonian effects of the Breit interaction as well as the QED effects were included in the different calculation methods. Several allowed transitions are calculated for the first time. Those transitions have been compared with other works such as experimental data published by NIST [12] and others [17,30], as well as theoretical data from Aggarwal *et al* [19]. A very good agreement obtained in most cases. In general, the best results are obtained with the MBPT method for the different calculated atomic parameters. The average relative deviations of energy levels and wavelengths obtained are around $0.46 \pm 0.11\%$ and $-0.47 \pm 0.9\%$ respectively, while the average relative deviations of weighted oscillator strengths and transition rates are around 1% and 2.06% respectively. Our results are useful for many applications such as thermonuclear fusion, laser and plasma physics as well as astrophysics.

Acknowledgements

This work has been realised with the financial support of the Tunisian Ministry of Higher Education and Scientific Research. SM and HJ would like to thank Sirine Ben Nasr and Dhia Elhak Salhi for their assistance.

References

[1] C Zhou, J Cao, L Liang, G Yu, Z Wang and H He, *Optik* **126**, 4105 (2015)
[2] S Manai, S B Nasr, D E Salhi and H Jelassi, *14th Arab Conference on the Peaceful Uses of Atomic Energy, Arab Republic of Egypt* (16–20 December 2018) Vol. 9
[3] D J Lennon, P L Dufton, A Hibbert and A E Kingston, *The Astrophys. J.* **294**, 200 (1985)
[4] F P Keenan, P L Dufton, W A Feibelman, K L Bell, A Hibbert and R P Stafford, *The Astrophys. J.* **423**, 882 (1994)
[5] S L Rao, A Sharma, M Kushwah, P Kalaria, T K Sharma, V Rathod, R Shah, D Mandge and G Joshi, *Fusion Sci. Technol.* **65**, 129 (2014)
[6] D E Salhi, P Quinet and H Jelassi, *At. Data Nucl. Data Tables* **126**, 70 (2019)
[7] S M McCann and F P Keenan, *Solar Phys.* **112**, 83 (1987)
[8] K P Dere, E Landi, P R Young and G Del Zanna, *The Astrophys. J. Suppl. Ser.* **134**, 331 (2001)
[9] A Litnovsky, V S Voitsenya, A Costley and A J H Donné, *Nuclear fusion* **47**, 833 (2007)
[10] L F Zakharov, W Blanchard, R Kaita, H Kugel, R Majeski and J Timberlake, *J. Nucl. Mater.* **363**, 453 (2007)
[11] A M Cantu, W H Parkinson, G Tondello and G P Tozz, *J. Opt. Soc. Am.* **67**, 1030 (1977)
[12] A Kramida, Yu Ralchenko, J Reader and NIST ASD Team (2020), NIST Atomic Spectra Database (ver. 5.8) (Online), Available: https://physics.nist.gov/asd (2021, February 5) (National Institute of Standards and Technology, Gaithersburg, MD), https://doi.org/10.18434/T4W30F
[13] S Diehl *et al*, *Phys. Rev. Lett.* **84**, 1677 (2000)
[14] G W F Drake, *Phys. Rev. A* **5**, 614 (1972)
[15] H-L Zhou and S T Manson, *J. Phys. B* **33**, L663 (2000)

[16] Głowacki Leszek, At. Data Nucl. Data Tables **133**, 101344 (2020)
[17] W A Wijngaarden and B Jian, *The Eur. Phys. J. Spec. Top*. **222**, 2057 (2013)
[18] B Sow, M Sow, Y Gning, A Traore, A S Ndao and A Wague, *Radiat. Phys. Chem.* **123**, 25 (2016)
[19] K M Aggarwal, T Kato, F P Keenan and I Murakami, *Phys. Scr.* **83**, 015302 (2010)
[20] M F Gu, *Can. J. Phys.* **86**, 675 (2008)
[21] S Hamasha and R Alshaiub, *Phys. Scr*. **86**, 065302 (2012)
[22] D E Salhi and H Jelassi, *Orient. J. Phys. Sci*. **2**, 2 (2017)
[23] M H Chen, K T Cheng, W R Johnson and J Sapirstein, *Phys. Rev. A* **52**, 266 (1995)
[24] D E Salhi and H Jelassi, *Can. J. Phys*. **96**, 343 (2017)
[25] R Si, X L Guo, J Yan, C Y Li, S Li, M Huang, C Y Chen, Y S Wang and Y M Zou, *J. Quant. Spectrosc. Radiat. Transfer* **163**, 7 (2015)
[26] S B Nasr, D E Salhi, P Quinet and H Jelassi, *At. Data Nucl. Data Tables* **129**, 101279 (2019)
[27] D Schürmann, *Z. Phys. A* **273**, 331 (1975)
[28] K M Aggarwal and F P Keenan, *Phys. Scr*. **85**, 025305 (2012)
[29] K M Aggarwal and F P Keenan, *Phys. Scr.* **89**, 125401 (2014)
[30] D Schurmann, D Haas, P H Heckmann and H Buttlar, *Phys. Lett. A* **42**, 27 (1972)